

REPORT DOCUMENTATION PAGE			Form Approved OMB NO. 0704-0188		
<p>The public reporting burden for this collection of information is estimated to average 1 hour per response, including the time for reviewing instructions, searching existing data sources, gathering and maintaining the data needed, and completing and reviewing the collection of information. Send comments regarding this burden estimate or any other aspect of this collection of information, including suggestions for reducing this burden, to Washington Headquarters Services, Directorate for Information Operations and Reports, 1215 Jefferson Davis Highway, Suite 1204, Arlington VA, 22202-4302. Respondents should be aware that notwithstanding any other provision of law, no person shall be subject to any penalty for failing to comply with a collection of information if it does not display a currently valid OMB control number.</p> <p>PLEASE DO NOT RETURN YOUR FORM TO THE ABOVE ADDRESS.</p>					
1. REPORT DATE (DD-MM-YYYY)		2. REPORT TYPE New Reprint		3. DATES COVERED (From - To) -	
4. TITLE AND SUBTITLE Free-Surface Flow and Fluid-Object Interaction Modeling With Emphasis on Ship Hydrodynamics			5a. CONTRACT NUMBER W911NF-11-1-0083		
			5b. GRANT NUMBER		
			5c. PROGRAM ELEMENT NUMBER 611102		
6. AUTHORS I. Akkerman, Y. Bazilevs, D. J. Benson, M. W. Farthing, C. E. Kees			5d. PROJECT NUMBER		
			5e. TASK NUMBER		
			5f. WORK UNIT NUMBER		
7. PERFORMING ORGANIZATION NAMES AND ADDRESSES University of California - San Diego Office of C & G Administration The Regents of the Univ. of Calif., U.C. San Diego La Jolla, CA 92093 -0934			8. PERFORMING ORGANIZATION REPORT NUMBER		
9. SPONSORING/MONITORING AGENCY NAME(S) AND ADDRESS(ES) U.S. Army Research Office P.O. Box 12211 Research Triangle Park, NC 27709-2211			10. SPONSOR/MONITOR'S ACRONYM(S) ARO		
			11. SPONSOR/MONITOR'S REPORT NUMBER(S) 57917-MA.4		
12. DISTRIBUTION AVAILABILITY STATEMENT Approved for public release; distribution is unlimited.					
13. SUPPLEMENTARY NOTES The views, opinions and/or findings contained in this report are those of the author(s) and should not be construed as an official Department of the Army position, policy or decision, unless so designated by other documentation.					
14. ABSTRACT This paper presents our approach for the computation of free-surface/rigid-body interaction phenomena with emphasis on ship hydrodynamics. We adopt the level set approach to capture the free-surface. The rigid body is described using six-degree-of-freedom equations of motion. An interface-tracking method is used to handle the interface between the moving rigid body and the fluid domain. An Arbitrary Lagrangian–Eulerian version of the residual-based variational multiscale formulation for the Navier–Stokes and level set equations is employed in					
15. SUBJECT TERMS flow, fluids, hydrodynamics, Navier-Stokes equations, shipbuilding industry, variational techniques					
16. SECURITY CLASSIFICATION OF:			17. LIMITATION OF ABSTRACT UU	15. NUMBER OF PAGES	19a. NAME OF RESPONSIBLE PERSON Yuri Bazilevs
a. REPORT UU	b. ABSTRACT UU	c. THIS PAGE UU			19b. TELEPHONE NUMBER 858-534-3663

## **Report Title**

Free-Surface Flow and Fluid-Object Interaction Modeling With Emphasis on Ship Hydrodynamics

### **ABSTRACT**

This paper presents our approach for the computation of free-surface/rigid-body interaction phenomena with emphasis on ship hydrodynamics. We adopt the level set approach to capture the free-surface. The rigid body is described using six-degree-of-freedom equations of motion. An interface-tracking method is used to handle the interface between the moving rigid body and the fluid domain. An Arbitrary Lagrangian–Eulerian version of the residual-based variational multiscale formulation for the Navier–Stokes and level set equations is employed in order to accommodate the fluid domain motion. The free-surface/rigid body problem is formulated and solved in a fully coupled fashion. The numerical results illustrate the accuracy and robustness of the proposed approach.



---

**REPORT DOCUMENTATION PAGE (SF298)**  
**(Continuation Sheet)**

---

Continuation for Block 13

ARO Report Number    57917.4-MA  
Free-Surface Flow and Fluid-Object Interaction M    ...

Block 13: Supplementary Note

© 2012 . Published in Journal of Applied Mechanics, Vol. Ed. 0 79, (1) (2012), (, (1). DoD Components reserve a royalty-free, nonexclusive and irrevocable right to reproduce, publish, or otherwise use the work for Federal purposes, and to authroize others to do so (DODGARS §32.36). The views, opinions and/or findings contained in this report are those of the author(s) and should not be construed as an official Department of the Army position, policy or decision, unless so designated by other documentation.

Approved for public release; distribution is unlimited.

## I. Akkerman

Coastal and Hydraulics Laboratory,  
US Army Engineer Research  
and Development Center,  
Vicksburg, MS 39180-6133;  
USA and Department of Structural Engineering,  
University of California, San Diego,  
La Jolla, CA 92093  
e-mail: iakkerman@ucsd.edu

## Y. Bazilevs

e-mail: jbazilevs@ucsd.edu

## D. J. Benson

Department of Structural Engineering,  
University of California, San Diego,  
La Jolla, CA 92093

## M. W. Farthing

## C. E. Kees

Coastal & Hydraulics Laboratory,  
US Army Engineer Research  
and Development Center,  
Vicksburg, MS 39180-6133

# Free-Surface Flow and Fluid-Object Interaction Modeling With Emphasis on Ship Hydrodynamics

*This paper presents our approach for the computation of free-surface/rigid-body interaction phenomena with emphasis on ship hydrodynamics. We adopt the level set approach to capture the free-surface. The rigid body is described using six-degree-of-freedom equations of motion. An interface-tracking method is used to handle the interface between the moving rigid body and the fluid domain. An Arbitrary Lagrangian–Eulerian version of the residual-based variational multiscale formulation for the Navier–Stokes and level set equations is employed in order to accommodate the fluid domain motion. The free-surface/rigid body problem is formulated and solved in a fully coupled fashion. The numerical results illustrate the accuracy and robustness of the proposed approach. [DOI: 10.1115/1.4005072]*

## 1 Introduction

Accurate prediction of wave loading on vessels and their motion necessitates the development of a simulation framework that involves free-surface flow and fluid-structure interaction (FSI) (see, for example, Ref. [1]). The simulation framework must be such that it is able to keep track of two types of interfaces: the air-water interface and the fluid-structure interface.

Depending on flow conditions, the free-surface motion may be smooth or violent, with wave breaking and other topological changes. As a result, the use of an interface-capturing method (see Ref. [2] for the terminology) is a convenient and practical choice for the proposed application. In this work, we make use of the level-set method to handle free-surface flow (see Refs. [3–5]). In the proposed methodology, the boundary between the two fluids is described implicitly as a zero level set of a scalar function defined in the problem domain. The subdomains corresponding to negative and positive values of the level set function are those occupied by air and water, respectively. The level set function is simultaneously a signed-distance function, meaning its magnitude at a point in 3D space is the distance from that point to the air-water interface, and its sign determines if the point is in the water or air domain. The signed distance property of the scalar function is not necessary in general; however, it has several accuracy benefits, as discussed in Ref. [6].

Simulating interaction of free-surface flow with moving and deformable structures requires additional computational technology that is able to track the interface between the structure and the surrounding air-water medium. Therefore, the Mixed Interface-Tracking/Interface-Capturing Technique (MITICT) is used to track the fluid-structure interface and to capture the air-water interface. The MITICT [7] was introduced primarily for fluid-object interactions with multiple fluids. The MITICT was success-

fully tested in Ref. [8], where the interface-tracking technique used was a space-time formulation [9,10], and the interface-capturing method was the Edge-Tracker Interface Locator Technique (ETILT) [7]. It was also tested in Ref. [11] by using a moving Lagrangian interface technique [12] for interface tracking and the ETILT for interface capturing. The interface-tracking technique used in the MITICT can also be the Arbitrary Lagrangian–Eulerian (ALE) method [13], which is employed in this work. In this paper we assume that the structures are complex-geometry six degree-of-freedom (6DOF) rigid objects. The extension to flexible structures will be pursued in future work.

The paper is outlined as follows. In Sec. 2, we present the governing equations of free-surface flow. In Sec. 3, we present our discrete free-surface formulation, which includes the Residual-based Variational Multiscale formulation (RBVMS) in ALE form, weak enforcement of essential boundary conditions, re-distancing, and restoration of the global fluid mass balance. The free-surface formulation is essentially that developed in Refs. [14,15]. In this section, we also present our rigid body dynamics and mesh motion formulations. In Sec. 4, we present our time integration method and solution strategy for the coupled problem. We advocate that the fluid and level set solutions are handled in a fully-coupled fashion, which significantly increases the robustness of the proposed methodology. We also present a novel time integration strategy for the rigid body equations, where the rotation matrix becomes an additional problem unknown that is integrated in time along with the displacement and rotational degrees of freedom. In Sec. 5, we present two numerical examples. The first one is the well-known MARIN dam break problem [14–18], which is a free-surface flow without fluid-object interaction. The problem is used to illustrate the effect of the penalty parameter in the level set re-distancing equations and the effect of using a strongly coupled Navier-Stokes/level set convection formulation. The second example consists of a DTMB 5415 Navy combatant at lab scale in head waves of large amplitude, which illustrates direct applicability of the proposed methodology to ship hydrodynamics simulations.

Contributed by the Applied Mechanics Division of ASME for publication in the JOURNAL OF APPLIED MECHANICS. Manuscript received March 22, 2011; final manuscript received May 15, 2011; published online December 13, 2011. Assoc. Editor: Tayfun E. Tezduyar.

## 2 Governing Equations of the Free-Surface Air-Water Modeling

In this section, we summarize the governing differential equations of free-surface flow on a moving spatial domain. Let  $\Omega_t \in \mathbb{R}^d$ ,  $d = 2, 3$  denote the combined air-water domain at current time  $t$  and let  $\Gamma_t$  be its boundary. The domain  $\Omega_t$  is decomposed into the water and air subdomains,  $\Omega_t^w$  and  $\Omega_t^a$ , respectively, and  $\Gamma_t^{aw}$  denotes the boundary between the air and water subdomains. See Fig. 1 for an illustration.

In this work we make use of the level set method to capture the air-water interface (see, e.g., Refs. [3–5]).

For this, we introduce a scalar function  $\phi(\mathbf{x}, t)$  and define:

$$\Omega_t^a = \{\mathbf{x} | \phi(\mathbf{x}, t) < 0, \quad \forall \mathbf{x} \in \Omega_t\} \quad (1)$$

$$\Omega_t^w = \{\mathbf{x} | \phi(\mathbf{x}, t) > 0, \quad \forall \mathbf{x} \in \Omega_t\} \quad (2)$$

$$\Gamma_t^{aw} = \{\mathbf{x} | \phi(\mathbf{x}, t) = 0, \quad \forall \mathbf{x} \in \Omega_t\} \quad (3)$$

In our modeling framework, the air and water domains will be distinguished by assigning the corresponding values to the fluid density and viscosity. Namely, we assume that the density,  $\rho$ , of the two-fluid air-water medium is given by:

$$\rho = \rho_w H(\phi) + \rho_a (1 - H(\phi)) \quad (4)$$

where  $\rho_w$  and  $\rho_a$  are the densities of water and air, respectively, and  $H(\phi)$  is the Heaviside function given by

$$H(\phi) = \begin{cases} 0 & \text{if } \phi < 0 \\ 1 & \text{if } \phi > 0 \end{cases} \quad (5)$$

Likewise, the combined dynamic viscosity,  $\mu$ , is given by:

$$\mu = \mu_w H(\phi) + \mu_a (1 - H(\phi)) \quad (6)$$

where  $\mu_w$  and  $\mu_a$  are the dynamic viscosities of water and air, respectively.

With this definition of the fluid material parameters, the Navier–Stokes equations of incompressible flow in the arbitrary Lagrangian–Eulerian (ALE) description take the form of:

$$\rho \left( \frac{\partial \mathbf{u}}{\partial t} \Big|_{\hat{\mathbf{x}}} + (\mathbf{u} - \hat{\mathbf{u}}) \cdot \nabla_{\hat{\mathbf{x}}} \mathbf{u} - \mathbf{f} \right) - \nabla_{\hat{\mathbf{x}}} \cdot \boldsymbol{\sigma} = 0 \quad (7)$$

$$\nabla_{\hat{\mathbf{x}}} \cdot \mathbf{u} = 0 \quad (8)$$

where the fluid Cauchy stress,  $\boldsymbol{\sigma}$ , is defined as:

$$\boldsymbol{\sigma}(\mathbf{u}, p) = -p\mathbf{I} + 2\mu \nabla_{\hat{\mathbf{x}}}^s \mathbf{u} \quad (9)$$

$\mathbf{u}$  and  $p$  are the fluid velocity and pressure,  $\mathbf{f}$  is the body force per unit mass,  $\hat{\mathbf{u}}$  is the velocity of the fluid domain, and  $\nabla^s$  is a symmetric gradient. In Eq. (7), the partial time derivative is taken

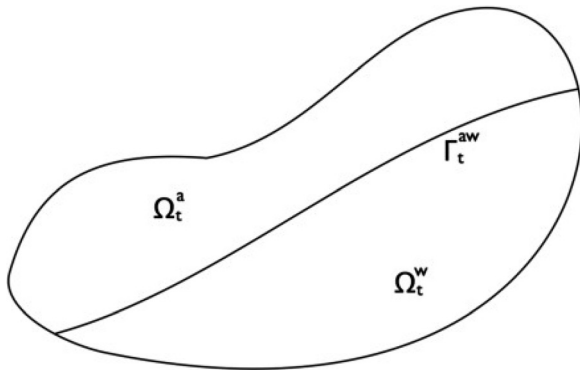


**Fig. 1** The fluid spatial domain decomposed into the water and air subdomains denoted by  $\Omega_t^w$  and  $\Omega_t^a$ , respectively. The air-water interface is denoted by  $\Gamma_t^{aw}$ .

with respect to a referential coordinate  $\hat{\mathbf{x}}$  held fixed. In Eqs. (7) and (8) the space derivatives are taken with respect to the current configuration spatial coordinates denoted by  $\mathbf{x}$ . We note that the fluid domain velocity is assumed to be completely independent of the velocity of the fluid material particles.

We assume that the air-water interface is moving with the fluid material particles, which we model by means of an additional convection equation for the level set  $\phi$  in the ALE description:

$$\frac{\partial \phi}{\partial t} \Big|_{\hat{\mathbf{x}}} + (\mathbf{u} - \hat{\mathbf{u}}) \cdot \nabla_{\hat{\mathbf{x}}} \phi = 0 \quad (10)$$

The above equations, with the associated boundary conditions constitute an air-water free surface formulation on a moving domain  $\Omega_t$  at the continuous level.

## 3 Discrete Formulation

**3.1 Discrete Formulation of the Two-Fluid Problem.** We discretize the Navier–Stokes and level set equations using the residual-based variational multi-scale (RBVMS) formulation. The RBVMS formulation was originally proposed in Ref. [19] and applied to a variety of situations involving fluid flow and fluid-structure interaction [20–28]. For a thorough derivation of the RBVMS formulation the reader is referred to these publications. The RBVMS formulation for free-surface flow was also developed in [14,15,18].

Let  $\mathcal{V}^h$  denote the discrete solution space for the velocity-pressure-level set triple  $\{\mathbf{u}^h, p^h, \phi^h\}$  and let  $\mathcal{W}^h$  denote the discrete weighting space for the linear momentum, continuity and level set equations  $\{\mathbf{w}^h, q^h, \eta^h\}$ . The RBVMS formulation of the free-surface equations on a moving domain may be stated as: Find  $\{\mathbf{u}^h, p^h, \phi^h\} \in \mathcal{V}^h$  such that  $\forall \{\mathbf{w}^h, q^h, \eta^h\} \in \mathcal{W}^h$ :

$$\begin{aligned} & \int_{\Omega_t} \mathbf{w}^h \cdot \rho \left( \frac{\partial \mathbf{u}^h}{\partial t} \Big|_{\hat{\mathbf{x}}} + (\mathbf{u}^h - \hat{\mathbf{u}}^h) \cdot \nabla_{\hat{\mathbf{x}}} \mathbf{u}^h - \mathbf{f} \right) d\Omega \\ & + \int_{\Omega_t} \nabla_{\hat{\mathbf{x}}} \mathbf{w}^h : \boldsymbol{\sigma}(\mathbf{u}^h, p^h) d\Omega - \int_{(\Gamma_h)_t} \mathbf{w}^h \cdot d\mathbf{h} \Gamma \\ & + \int_{\Omega_t} q^h \nabla_{\hat{\mathbf{x}}} \cdot \mathbf{u}^h d\Omega \\ & + \int_{\Omega_t} \tau_M \left( (\mathbf{u}^h - \hat{\mathbf{u}}^h) \cdot \nabla_{\hat{\mathbf{x}}} \mathbf{w}^h + \frac{\nabla_{\hat{\mathbf{x}}} q^h}{\rho} \right) \cdot \mathbf{r}_M(\mathbf{u}^h, p^h) d\Omega \\ & + \int_{\Omega_t} \rho \tau_C \nabla_{\hat{\mathbf{x}}} \cdot \mathbf{w}^h r_C(\mathbf{u}^h, p^h) d\Omega \\ & - \int_{\Omega_t} \tau_M \mathbf{w}^h \cdot (\mathbf{r}_M(\mathbf{u}^h, p^h) \cdot \nabla_{\hat{\mathbf{x}}} \mathbf{u}^h) d\Omega \\ & - \int_{\Omega_t} \frac{\nabla_{\hat{\mathbf{x}}} \mathbf{w}^h}{\rho} : (\tau_M \mathbf{r}_M(\mathbf{u}^h, p^h)) \otimes (\tau_M \mathbf{r}_M(\mathbf{u}^h, p^h)) d\Omega \\ & + \int_{\Omega_t} \eta^h \left( \frac{\partial \phi^h}{\partial t} \Big|_{\hat{\mathbf{x}}} + (\mathbf{u}^h - \hat{\mathbf{u}}^h) \cdot \nabla_{\hat{\mathbf{x}}} \phi^h \right) d\Omega \\ & + \int_{\Omega_t} \tau_\phi (\mathbf{u}^h - \hat{\mathbf{u}}^h) \cdot \nabla_{\hat{\mathbf{x}}} \eta^h \left( \frac{\partial \phi^h}{\partial t} \Big|_{\hat{\mathbf{x}}} + (\mathbf{u}^h - \hat{\mathbf{u}}^h) \cdot \nabla_{\hat{\mathbf{x}}} \phi^h \right) d\Omega = 0 \end{aligned} \quad (11)$$

In Eq. (11) all the integrals are taken element-wise,  $\mathbf{r}_M(\mathbf{u}^h, p^h)$  and  $r_C(\mathbf{u}^h, p^h)$  are the element-level residuals of the momentum and continuity equations given by the following:

$$\mathbf{r}_M(\mathbf{u}, p) = \rho \left( \frac{\partial \mathbf{u}}{\partial t} \Big|_{\hat{\mathbf{x}}} + (\mathbf{u} - \hat{\mathbf{u}}) \cdot \nabla_{\hat{\mathbf{x}}} \mathbf{u} - \mathbf{f} \right) - \nabla_{\hat{\mathbf{x}}} \cdot \boldsymbol{\sigma}(\mathbf{u}, p) \quad (12)$$

$$r_c(\mathbf{u}, p) = \nabla_x \cdot \mathbf{u} \quad (13)$$

and the  $\tau$ 's are the stabilization parameters discussed in the sequel.

In the presence of solid walls, (e.g., the ship hull), it is beneficial to augment the coupled weak formulation given by Eq. (11) with additional terms that give rise to weak enforcement of essential boundary conditions. In this case, the left-hand side of Eq. (11) is augmented with the following terms:

$$\begin{aligned} & - \int_{(\Gamma_g)_t} \mathbf{w}^h \cdot \boldsymbol{\sigma}(\mathbf{u}^h, p^h) \mathbf{n} d\Gamma \\ & - \int_{(\Gamma_g)_t} (2\mu \nabla_x \mathbf{w}^h \mathbf{n} + q^h \mathbf{n}) \cdot (\mathbf{u}^h - \mathbf{u}_g) d\Gamma \\ & - \int_{(\Gamma_g)_t} \mathbf{w}^h \cdot ((\mathbf{u}^h - \hat{\mathbf{u}}^h) \cdot \mathbf{n}) (\mathbf{u}^h - \mathbf{u}_g) d\Gamma \\ & + \int_{(\Gamma_g)_t} \tau_B \mathbf{w}^h \cdot (\mathbf{u}^h - \mathbf{u}_g) d\Gamma \end{aligned} \quad (14)$$

where  $\mathbf{u}_g$  is the prescribed fluid velocity on  $(\Gamma_g)_t$ , the Dirichlet portion of the fluid domain boundary, and  $(\Gamma_g)_t^-$  denotes the “inflow” part of  $(\Gamma_g)_t$ . We refer the readers to Refs. [22,23,29] for the derivation and discussion of weak boundary conditions for the equations of fluid mechanics.  $\tau_B$  is the boundary stabilization or penalty parameter.

For flows at very high Reynolds number, as well as for pure convection, the RBVMS framework alone may not be sufficiently robust. In this case, additional discontinuity-capturing terms may be added to the left-hand side of Eq. (11)

$$+ \int_{\Omega_t} \nabla_x \mathbf{w}^h \boldsymbol{\kappa}_{ns} \nabla_x \mathbf{u}^h d\Omega \quad (15)$$

$$+ \int_{\Omega_t} \nabla_x \eta^h \boldsymbol{\kappa}_{ls} \nabla_x \phi^h d\Omega \quad (16)$$

where  $\boldsymbol{\kappa}_{ns}$  and  $\boldsymbol{\kappa}_{ls}$  are tensor-valued, residual-based, discontinuity-capturing viscosities.

The density and viscosity of the two-fluid system in the discrete setting are computed as:

$$\rho = \rho_w H_\varepsilon(\phi^h) + \rho_a (1 - H_\varepsilon(\phi^h)) \quad (17)$$

$$\mu = \mu_w H_\varepsilon(\phi^h) + \mu_a (1 - H_\varepsilon(\phi^h)) \quad (18)$$

where  $H_\varepsilon$  is the *regularized Heaviside function*. In this work, we take:

$$H_\varepsilon(\phi) = \begin{cases} 0 & \text{if } \phi \leq -\varepsilon \\ \frac{1}{2} \left( 1 + \frac{\phi}{\varepsilon} + \frac{1}{\pi} \sin\left(\frac{\phi\pi}{\varepsilon}\right) \right) & \text{if } |\phi| < \varepsilon \\ 1 & \text{if } \phi \geq \varepsilon \end{cases} \quad (19)$$

where  $\varepsilon \sim O(h)$  defines the interface width between the air and water subdomains. Note that  $\varepsilon \rightarrow 0$  as the mesh is refined.

Regularization of the Heaviside function places the requirement on the level set function  $\phi^h$  to maintain the *signed distance property*. This means that the value of  $\phi^h$  at a point  $\mathbf{x}$  at time  $t$  is the perpendicular distance of that point to the air-water interface  $\Gamma_t^{aw}$ . In the water domain, the distance takes on a positive value, while in the air domain it is negative. To enforce the signed distance property of the level set function, we define  $\phi_d^h$  such that:

$$\|\nabla_x \phi_d^h\| = 1 \text{ in } \Omega_t \quad (20)$$

$$\phi_d^h = 0 \text{ on } \Gamma_t^{aw} \quad (21)$$

in a weak sense. Equation (20) is the Eikonal partial differential equation subject to the interior constraint given by Eq. (21). To

satisfy Eqs. (20)–(21), we introduce a “pseudo-time” variable  $\tilde{t}$  and integrate the following semi-discrete variational equation in pseudo-time: Given  $\phi^h(\mathbf{x}, t)$ , find  $\phi_d^h \in \mathcal{V}_s^h$ , such that  $\forall \eta^h \in \mathcal{W}_s^h$ :

$$\begin{aligned} & \int_{\Omega_t} \eta^h \left( \frac{\partial \phi_d^h}{\partial \tilde{t}} + \mathbf{a} \cdot \nabla_x \phi_d^h - S_\varepsilon(\phi^h) \right) d\Omega \\ & + \int_{\Omega_t} \tau_{\phi_d} \mathbf{a} \cdot \nabla_x \eta^h \left( \frac{\partial \phi_d^h}{\partial \tilde{t}} + \mathbf{a} \cdot \nabla_x \phi_d^h - S_\varepsilon(\phi^h) \right) d\Omega = 0 \end{aligned} \quad (22)$$

where

$$\mathbf{a} = S_\varepsilon(\phi^h) \frac{\nabla_x \phi_d^h}{\|\nabla_x \phi_d^h\|} \quad (23)$$

and

$$S_\varepsilon(\phi) = 2H_\varepsilon(\phi) - 1 \quad (24)$$

are an effective “convection” velocity and a regularized sign function, respectively.

The formulation given by Eq. (22) is the SUPG method [30] applied to the Eikonal equation. At the steady state, the above problem produces a new level set field  $\phi_d$  with the signed distance property and zero level set coincident with that of  $\phi$ . This re-distancing approach was first proposed in Ref. [4], and employed in Refs. [5,14,15] for finite element computations of free surface phenomena.

To prevent excessive motions of the air-water interface during the re-distancing procedure, we recommend adding a penalty term to the left-hand side of Eq. (22) of the form:

$$+ \int_{\Omega_t} \eta^h \lambda_{pen} H'_\varepsilon(\phi^h) (\phi_d^h - \phi^h) d\Omega \quad (25)$$

In the above penalty term, the constant parameter  $\lambda_{pen}$  is multiplied by  $H'_\varepsilon(\phi_d^h)$ , which scales as  $1/h$  in the interface layer rendering the equations dimensionally consistent. Furthermore,  $H'_\varepsilon(\phi_d^h)$  is identically zero away from the interface; hence the term is only active where it is necessary. In Sec. 5.1.1, the importance of this term will be clearly demonstrated.

Both convection and re-distancing of the level set may result in the loss or gain of the total fluid mass. The amount of mass deficit depends on many factors. One is more likely to significantly upset the mass balance on a coarse problem mesh than on a fine problem mesh. Significant mass loss or gain may also occur when the discrete equations are integrated for a long time period. In this case, seemingly minor mass errors for a given time step may compound into a large mass error at the end of the computation. As a result, a mass correction procedure is necessary. We begin with a global mass balance law for a moving domain, which reads:

$$\frac{d}{dt} \int_{\Omega_t} \rho d\Omega + \int_{\Gamma_t} \rho(\mathbf{u} - \hat{\mathbf{u}}) \cdot \mathbf{n} d\Gamma = 0 \quad (26)$$

We integrate Eq. (26) in time over the time step  $(t_n, t_{n+1})$  and approximate the term corresponding to the boundary integral using a midpoint rule to obtain:

$$\begin{aligned} & \int_{\Omega_{n+1/2}} \rho_{n+1} d\Omega - \int_{\Omega_n} \rho_n d\Omega \\ & + \Delta t_n \int_{\Gamma_{n+1/2}} \rho_{n+1/2} (\mathbf{u}_{n+1/2} - \hat{\mathbf{u}}_{n+1/2}) \cdot \mathbf{n}_{n+1/2} d\Gamma = 0 \end{aligned} \quad (27)$$

which is a time discrete version of the mass balance equation. To ensure mass balance at  $t_{n+1}$ , we perturb the newly re-distanced level set function  $\phi_d^h$  by a *global constant* such that Eq. (27) is

satisfied for the regularized fluid density  $\rho$  given by Eq. (17). This procedure ensures the global mass balance at every time step. To achieve mass balance also in a local sense, a procedure proposed in Ref. [14] may be employed instead.

**3.1.1 Computation of Mesh-Dependent Parameters.** To define the method parameters that depend on the mesh size, we first define the element metric tensor as:

$$\mathbf{G} = \frac{\partial \xi^T}{\partial \mathbf{x}} \frac{\partial \xi}{\partial \mathbf{x}} \quad (28)$$

where  $\mathbf{x}$  and  $\xi$  are the coordinates of the physical element and its parametric counterpart, respectively.

The RBVMS formulation parameters  $\tau_M$ ,  $\tau_C$  and  $\tau_\phi$  in Eq. (11) are defined as (see Ref. [27])

$$\tau_M = \left( \frac{4}{\Delta t^2} + (\mathbf{u}^h - \hat{\mathbf{u}}^h) \cdot \mathbf{G}(\mathbf{u}^h - \hat{\mathbf{u}}^h) + C_I \left( \frac{\mu}{\rho} \right)^2 \mathbf{G} : \mathbf{G} \right)^{-1/2} \quad (29)$$

$$\tau_C = (\text{tr} \mathbf{G} \tau_M)^{-1} \quad (30)$$

$$\tau_\phi = \left( \frac{4}{\Delta t^2} + (\mathbf{u}^h - \hat{\mathbf{u}}^h) \cdot \mathbf{G}(\mathbf{u}^h - \hat{\mathbf{u}}^h) \right)^{-1/2} \quad (31)$$

where  $C_I$  is the constant emanating from the element-wise inverse estimate (see Ref. [31]). The stabilization parameter  $\tau_{\phi_d}$  in Eq. (22) is given by:

$$\tau_{\phi_d} = \left( \frac{4}{\Delta t^2} + \mathbf{a} \cdot \mathbf{G} \mathbf{a} \right)^{-1/2} \quad (32)$$

The penalty parameter in the weak Dirichlet BC formulation  $\tau_B$  is given by (see Ref. [22])

$$\tau_B = C_I^b \mu \sqrt{\mathbf{n} \cdot \mathbf{G} \mathbf{n}} \quad (33)$$

where  $C_I^b$  is a constant emanating from the boundary inverse estimate. An alternative definition of  $\tau_B$  that is based on the wall function ideas may be found in Ref. [23].

The discontinuity capturing parameters in Eqs. (15)–(16) are given by:

$$\begin{aligned} \kappa_{ns} &= C_{ns} \frac{\|\mathbf{r}_M(\mathbf{u}^h, p^h)\|}{u_{ref} \sqrt{\mathbf{G} : \mathbf{G}}} \mathbf{I} \\ \kappa_{ls} &= C_{ls} \frac{\left\| \frac{\partial \phi^h}{\partial t} \right\|_{\hat{\mathbf{x}}} + (\mathbf{u}^h - \hat{\mathbf{u}}^h) \cdot \nabla_x \phi^h}{\sqrt{\nabla_x \phi^h \cdot \mathbf{G} \nabla_x \phi^h}} \mathbf{I} \end{aligned} \quad (34)$$

where  $C_{ns}$  and  $C_{ls}$  are positive constants and  $u_{ref}$  is a reference value of flow speed (e.g., magnitude of inflow velocity). Note that the discontinuity-capturing parameters are residual-based and isotropic.  $\kappa_{ns}$  is a modified version of the YZ- $\beta$  discontinuity capturing proposed in Refs. [32,33] corresponding to  $\beta = 2$ , which is the least intrusive definition. The definition of  $\kappa_{ls}$  corresponds to the CAU discontinuity capturing proposed in Ref. [34], and may also be obtained by setting  $\beta = 1$  in the scalar version of the YZ- $\beta$  discontinuity capturing method. Alternative definitions of discontinuity-capturing terms, which are not residual based, can be found in Ref. [35] in the context of incompressible flows and in Ref. [36] in the context of incompressible flows with thermal coupling.

Finally, we define the *local* interface half-width  $\varepsilon$  as:

$$\varepsilon = \alpha \frac{\|\nabla_x \phi^h\|}{\sqrt{\nabla_x \phi^h \cdot \mathbf{G} \nabla_x \phi^h}} \quad (35)$$

where  $\alpha$  is an integer parameter corresponding to the number of elements used across the air-water interface. This definition of  $\varepsilon$  is

used to regularize the fluid density and viscosity in Eqs. (17)–(18). The structure of Eq. (35) gives the interface half-width in the direction of  $\nabla_x \phi^h$ , which is orthogonal to the interface, as desired.

Note that all the mesh-dependent parameters are defined in terms of the element metric tensor  $\mathbf{G}$ , which automatically accounts for element topology. Alternative definitions of stabilization and discontinuity-capturing parameters are possible and may be found in Refs. [26,33,37–39].

**3.2 Rigid Body Dynamics Formulation.** We begin with the definition of the rigid body kinematics. Let  $\Omega_0$  denote the reference configuration of the rigid object and let  $\Omega_t$  denote its current configuration. Let  $\mathbf{X}$  denote the reference configuration coordinates of the rigid body and let  $\mathbf{x}$  denote the current configuration coordinates of the rigid body. The rigid body kinematics is composed of translation and rotational motions and may be summarized as:

$$\mathbf{x} = \mathbf{Q}(\mathbf{X} - \mathbf{X}_0) + \mathbf{X}_0 + \mathbf{d}_0 \quad (36)$$

where  $\mathbf{Q}$  is a rotation matrix,  $\mathbf{X}_0$  is a center of mass, and  $\mathbf{d}_0$  is the displacement of the mass center. From Eq. (36) we obtain the rigid body displacement and velocity fields as:

$$\mathbf{d} = (\mathbf{Q} - \mathbf{I})(\mathbf{X} - \mathbf{X}_0) + \mathbf{d}_0 \quad (37)$$

and

$$\dot{\mathbf{d}} = \dot{\mathbf{Q}}(\mathbf{X} - \mathbf{X}_0) + \dot{\mathbf{d}}_0 \quad (38)$$

respectively.

Let  $\mathbf{x}_0 = \mathbf{X}_0 + \mathbf{d}_0$  denote the rigid body center of mass in the current configuration. Substituting Eq. (36) in Eq. (38), the velocity field may be expressed in terms of current coordinates as:

$$\dot{\mathbf{d}} = \dot{\mathbf{Q}}\mathbf{Q}^{-1}(\mathbf{x} - \mathbf{x}_0) + \dot{\mathbf{d}}_0 = \boldsymbol{\Omega}(\mathbf{x} - \mathbf{x}_0) + \dot{\mathbf{d}}_0 \quad (39)$$

where

$$\boldsymbol{\Omega} = \dot{\mathbf{Q}}\mathbf{Q}^{-1} = \begin{bmatrix} 0 & -\omega_3 & \omega_2 \\ \omega_3 & 0 & -\omega_1 \\ -\omega_2 & \omega_1 & 0 \end{bmatrix} \quad (40)$$

is a skew-symmetric tensor of angular velocities. Note that, from Eq. (40),

$$\dot{\mathbf{Q}} = \boldsymbol{\Omega}\mathbf{Q} \quad (41)$$

which is a key relationship that we will employ in what follows. Since  $\boldsymbol{\Omega}$  is skew-symmetric, it has the axial vector  $\boldsymbol{\omega}$  given by:

$$\boldsymbol{\omega} = \begin{bmatrix} \omega_1 \\ \omega_2 \\ \omega_3 \end{bmatrix} \quad (42)$$

and the rigid body velocity field given by Eq. (39) may also be written as:

$$\dot{\mathbf{d}} = \boldsymbol{\omega} \times (\mathbf{x} - \mathbf{x}_0) + \dot{\mathbf{d}}_0 \quad (43)$$

In 3D, the translational velocities,  $\dot{\mathbf{d}}_0$ , and rotational velocities,  $\boldsymbol{\omega}$ , are the six degrees-of-freedom that define the kinematics of rigid body motion.

The dynamics of the rigid body is governed by the equations of balance of global linear and angular momentum, namely,

$$\frac{d}{dt} \int_{\Omega} \rho \dot{\mathbf{d}} d\Omega = \mathbf{F} \quad (44)$$

$$\frac{d}{dt} \int_{\Omega} (\mathbf{x} - \mathbf{x}_0) \times \rho \dot{\mathbf{d}} d\Omega = \mathbf{M} \quad (45)$$

where  $\mathbf{F}$  and  $\mathbf{M}$  are the global force and moment vectors acting on a rigid body and defined by

$$\mathbf{F} = m\mathbf{g} + \int_{\Gamma_i} \mathbf{h} d\Gamma \quad (46)$$

$$\mathbf{M} = \int_{\Gamma_i} (\mathbf{x} - \mathbf{x}_0) \times \mathbf{h} d\Gamma \quad (47)$$

$m = \int_{\Omega} \rho d\Omega$  is the mass of the object,  $\mathbf{g}$  is the gravity vector, and  $\mathbf{h}$  is the traction vector exerted on the object by an external medium. In this case,  $\mathbf{h}$  is the fluid traction vector.

Introducing the rigid body kinematics into the linear and angular momentum balance equations, we obtain the following system of six ordinary differential equations,

$$\frac{d}{dt} (m\dot{\mathbf{d}}_0) = \mathbf{F} \quad (48)$$

$$\frac{d}{dt} (\mathbf{J}_t \omega) = \mathbf{M} \quad (49)$$

where  $\mathbf{J}_t$  is the inertia tensor in the current configuration given by

$$\mathbf{J}_t = \mathbf{Q} \mathbf{J}_0 \mathbf{Q}^T \quad (50)$$

with  $\mathbf{J}_0$  being the inertia tensor in the reference configuration defined as

$$\mathbf{J}_0 = \int_{\Omega_0} \rho (\mathbf{X} - \mathbf{X}_0) \cdot (\mathbf{X} - \mathbf{X}_0) \mathbf{I} d\Omega - \int_{\Omega_0} \rho (\mathbf{X} - \mathbf{X}_0) \otimes (\mathbf{X} - \mathbf{X}_0) d\Omega \quad (51)$$

Note that  $\mathbf{J}_0$  is a function of the reference configuration quantities only, and may be computed once and for all for a given rigid object.

**3.3 Motion of the Fluid Domain.** In the MITICT framework, while the air-water interface is captured on the mesh that does not conform to it, the fluid-rigid object interface is tracked with a conforming mesh. For this, the computed rigid object displacement and velocity (see Eqs. (37) and (38)) are imposed as boundary conditions for the motion of the fluid domain mesh. The fluid mesh displacement in the interior of the fluid domain is found using the equations of linear elastostatics: Find  $\hat{\mathbf{d}}^h(t)$  such that  $\forall \hat{\mathbf{w}}^h$

$$\begin{aligned} \int_{\Omega_t} \nabla_{\hat{\mathbf{x}}} \hat{\mathbf{w}}^h 2\mu^h \nabla_{\hat{\mathbf{x}}} (\hat{\mathbf{d}}^h(t) - \hat{\mathbf{d}}^h(\tilde{t})) d\Omega \\ + \int_{\Omega_t} \nabla_{\hat{\mathbf{x}}} \cdot \hat{\mathbf{w}}^h \lambda^h \nabla_{\hat{\mathbf{x}}} \cdot (\hat{\mathbf{d}}^h(t) - \hat{\mathbf{d}}^h(\tilde{t})) d\Omega = 0 \end{aligned} \quad (52)$$

In Eq. (52)  $\hat{\mathbf{d}}^h(\tilde{t})$  and  $\Omega_{\tilde{t}}$  are the mesh displacement and mesh configuration at  $\tilde{t} < t$ , both considered known. In practice, we take  $\Omega_{\tilde{t}}$  to be the configuration at the previous time step. This renders the mesh motion problem linear in the unknown displacement variable  $\hat{\mathbf{d}}^h(t)$ . Also in Eq. (52)  $\mu^h$  and  $\lambda^h$  are the mesh Lamé parameters chosen to be:

$$\mu^h = \frac{E_m^h}{2(1 + \nu_m)} \quad (53)$$

$$\lambda^h = \frac{\nu_m E_m^h}{(1 + \nu_m)(1 - 2\nu_m)} \quad (54)$$

where  $E_m^h$ , the mesh Young's modulus, is given by:

$$E_m^h = E_m J_{x\xi}^{-1} \quad (55)$$

$J_{x\xi}$  is the Jacobian determinant of the isoparametric element mapping, and  $E_m$  and  $\nu_m$  are the constant, user-prescribed nominal mesh Young's modulus and Poisson ratio. We typically take  $E_m = 1$  and  $\nu_m = 0.3$ . The above procedure represents the so-called Jacobian stiffening method (see Ref. [40]), which preserves good mesh quality in the simulation. In particular, the small elements, which are usually placed near the fluid-object interface, become "stiffer" and are less likely to deform as much as the larger elements, which are typically placed in the areas where the solution is not expected to exhibit complex behavior.

## 4 Time Integration of the Free-Surface Fluid-Object Interaction Equations

In this section we present our time integration algorithm for the coupled free-surface fluid-object interaction problem. We make use of the generalized- $\alpha$  time integration method (see Refs. [41,42]) for the free-surface and mesh motion equations. The rigid body equations are integrated with a midpoint method. The latter choice will become clear in the sequel.

The generalize- $\alpha$  method applied to the coupled free-surface fluid-object interaction problem may be recast in the form of a three-stage predictor-multicorrector algorithm as follows.

Given  $\mathbf{u}_n, \dot{\mathbf{u}}_n, \mathbf{p}_n$ , the fluid velocity, its time derivative, and pressure nodal degrees of freedom, respectively,  $\phi_n, \dot{\phi}_n$ , the level set and its time derivative nodal degrees of freedom, respectively,  $(\mathbf{d}_0)_n, (\dot{\mathbf{d}}_0)_n$ ,  $\omega_n, \mathbf{Q}_n$ , the rigid body center of mass displacement and velocity, angular velocity, and the rotation matrix, respectively, and  $\hat{\mathbf{d}}_n, \hat{\mathbf{u}}_n, \hat{\mathbf{u}}_n$  the mesh displacement, velocity and acceleration nodal degrees of freedom, respectively, at time level  $t_n$ , find the corresponding quantities at time level  $t_{n+1}$  by executing the following stages:

**Predictor stage.** Initialize:

$$\mathbf{u}_{n+1,(0)} = \mathbf{u}_n$$

$$\dot{\mathbf{u}}_{n+1,(0)} = \frac{\gamma - 1}{\gamma} \dot{\mathbf{u}}_n$$

$$\mathbf{p}_{n+1,(0)} = \mathbf{p}_n$$

$$\phi_{n+1,(0)} = \phi_n$$

$$\dot{\phi}_{n+1,(0)} = \frac{\gamma - 1}{\gamma} \dot{\phi}_n$$

$$\hat{\mathbf{u}}_{n+1,(0)} = \hat{\mathbf{u}}_n$$

$$\hat{\mathbf{u}}_{n+1,(0)} = \frac{\gamma - 1}{\gamma} \hat{\mathbf{u}}_n$$

$$\hat{\mathbf{d}}_{n+1,(0)} = \hat{\mathbf{d}}_n + \Delta t \hat{\mathbf{u}}_n + \frac{\Delta t^2}{2} ((1 - 2\beta) \hat{\mathbf{u}}_n + 2\beta \hat{\mathbf{u}}_{n+1,(0)})$$

The subscript 0 on the left-hand side quantities is the iteration index, which is set to 0 at the predictor stage.

**Multicorrector stage.** Repeat the following iterations for  $l = 1, 2, \dots, l_{max}$ , where  $l$  is the iteration index and  $l_{max}$  is the maximum allowable number of nonlinear iterations set for this time step:

1. (a) Evaluate iterates at the intermediate time levels as:

$$\begin{aligned} \mathbf{u}_{n+\alpha_f,l} &= \mathbf{u}_n + \alpha_f (\mathbf{u}_{n+1,(l-1)} - \mathbf{u}_n) \\ \dot{\mathbf{u}}_{n+\alpha_f,l} &= \dot{\mathbf{u}}_n + \alpha_m (\dot{\mathbf{u}}_{n+1,(l-1)} - \dot{\mathbf{u}}_n) \\ \phi_{n+\alpha_f,l} &= \phi_n + \alpha_f (\phi_{n+1,(l-1)} - \phi_n) \\ \dot{\phi}_{n+\alpha_m,l} &= \dot{\phi}_n + \alpha_m (\dot{\phi}_{n+1,(l-1)} - \dot{\phi}_n) \\ \mathbf{d}_{n+\alpha_f,l} &= \mathbf{d}_n + \alpha_f (\mathbf{d}_{n+1,(l-1)} - \mathbf{d}_n) \\ \dot{\mathbf{d}}_{n+\alpha_f,l} &= \dot{\mathbf{d}}_n + \alpha_m (\dot{\mathbf{d}}_{n+1,(l-1)} - \dot{\mathbf{d}}_n) \end{aligned} \quad (56)$$

(b) Use the intermediate solutions to assemble  $\mathbf{R}^{mom}$ ,  $\mathbf{R}^{con}$ , and  $\mathbf{R}^{ls}$ , the discrete residuals of the momentum, continuity and level-set equations, and the corresponding matrices of the linear equation system,

$$\begin{aligned} \frac{\partial \mathbf{R}^{mom}}{\partial \dot{\mathbf{u}}_{n+1}} \Delta \dot{\mathbf{u}} + \frac{\partial \mathbf{R}^{mom}}{\partial \mathbf{p}_{n+1}} \Delta \mathbf{p} + \frac{\partial \mathbf{R}^{mom}}{\partial \dot{\phi}_{n+1}} \Delta \dot{\phi} &= -\mathbf{R}_{(l)}^{mom} \\ \frac{\partial \mathbf{R}^{con}}{\partial \dot{\mathbf{u}}_{n+1}} \Delta \dot{\mathbf{u}} + \frac{\partial \mathbf{R}^{con}}{\partial \mathbf{p}_{n+1}} \Delta \mathbf{p} + \frac{\partial \mathbf{R}^{con}}{\partial \dot{\phi}_{n+1}} \Delta \dot{\phi} &= -\mathbf{R}_{(l)}^{con} \\ \frac{\partial \mathbf{R}^{ls}}{\partial \dot{\mathbf{u}}_{n+1}} \Delta \dot{\mathbf{u}} + \frac{\partial \mathbf{R}^{ls}}{\partial \dot{\phi}_{n+1}} \Delta \dot{\phi} &= -\mathbf{R}_{(l)}^{ls} \end{aligned}$$

Solve this linear system using a preconditioned GMRES algorithm (see Ref. [43]) to a specified tolerance. We note that the left-hand side matrix couples the fluid and level set degrees of freedom. This strong coupling between the fluid and level set equations allows us to use larger time step sizes without the risk of encountering an instability associated with staggered approaches in which the fluid solve is followed by a level set solve.

(c) Update the fluid and level set solution as:

$$\begin{aligned} \dot{\mathbf{u}}_{n+1,(l)} &= \dot{\mathbf{u}}_{n+1,(l)} + \Delta \dot{\mathbf{u}} \\ \mathbf{u}_{n+1,(l)} &= \mathbf{u}_{n+1,(l)} + \gamma \Delta t \Delta \dot{\mathbf{u}} \\ \mathbf{p}_{n+1,(l)} &= \mathbf{p}_{n+1,(l)} + \Delta \mathbf{p} \\ \dot{\phi}_{n+1,(l)} &= \dot{\phi}_{n+1,(l)} + \Delta \dot{\phi} \\ \phi_{n+1,(l)} &= \phi_{n+1,(l)} + \gamma \Delta t \Delta \dot{\phi} \end{aligned} \quad (57)$$

2 (a) Evaluate the updated fluid solution at the half-step as:

$$\begin{aligned} \mathbf{u}_{n+\frac{1}{2},(l)} &= \frac{1}{2} (\mathbf{u}_n + \mathbf{u}_{n+1,(l)}) \\ \dot{\mathbf{u}}_{n+\frac{1}{2},(l)} &= \frac{1}{2} (\dot{\mathbf{u}}_n + \dot{\mathbf{u}}_{n+1,(l)}) \\ \phi_{n+\frac{1}{2},(l)} &= \frac{1}{2} (\phi_n + \phi_{n+1,(l)}) \\ \dot{\phi}_{n+\frac{1}{2},(l)} &= \frac{1}{2} (\dot{\phi}_n + \dot{\phi}_{n+1,(l)}) \\ \hat{\mathbf{d}}_{n+\frac{1}{2},(l)} &= \frac{1}{2} (\hat{\mathbf{d}}_n + \hat{\mathbf{d}}_{n+1,(l)}) \\ \hat{\mathbf{u}}_{n+\frac{1}{2},(l)} &= \frac{1}{2} (\hat{\mathbf{u}}_n + \hat{\mathbf{u}}_{n+1,(l)}) \end{aligned} \quad (58)$$

(b) Use the half-step fluid solution to assemble the  $\mathbf{F}^{n+1/2}$  and  $\mathbf{M}^{n+1/2}$ , force and moment load on the rigid object, respectively, using Eqs. (46) and (47). Using these loads, we solve the following discrete rigid body equations for  $(\mathbf{d}_0)_{n+1,(l)}$ ,  $(\dot{\mathbf{d}}_0)_{n+1,(l)}$ ,  $\boldsymbol{\omega}_{n+1,(l)}$ , and  $\mathbf{Q}_{n+1,(l)}$ :

$$m \frac{(\dot{\mathbf{d}}_0)_{n+1,(l)} - (\dot{\mathbf{d}}_0)_n}{\Delta t} = \mathbf{F}^{n+1/2} \quad (59)$$

$$\frac{(\mathbf{d}_0)_{n+1,(l)} - (\mathbf{d}_0)_n}{\Delta t} = \frac{1}{2} ((\dot{\mathbf{d}}_0)_{n+1,(l)} + (\dot{\mathbf{d}}_0)_n) \quad (60)$$

$$\frac{\mathbf{J}_{n+1,(l)} \boldsymbol{\omega}_{n+1,(l)} - \mathbf{J}_n \boldsymbol{\omega}_n}{\Delta t} = \mathbf{M}^{n+1/2} \quad (61)$$

$$\frac{\mathbf{Q}_{n+1,(l)} - \mathbf{Q}_n}{\Delta t} = \frac{1}{4} (\boldsymbol{\Omega}_{n+1,(l)} + \boldsymbol{\Omega}_n) (\mathbf{Q}_{n+1,(l)} + \mathbf{Q}_n) \quad (62)$$

where Eq. (50) is used to evaluate the inertia tensor  $\mathbf{J}_{n+1,(l)}$  as:

$$\mathbf{J}_{n+1,(l)} = \mathbf{Q}_{n+1,(l)} \mathbf{J}_0 \mathbf{Q}_{n+1,(l)}^T \quad (63)$$

Note that Eqs. (61)–(63) are nonlinear and coupled, requiring iteration. We solve Eq. (61) first, where we lag the inertia tensor. We solve Eq. (62) next and use the new rotation matrix to update the inertia tensor in Eq. (63). This procedure gives convergence in a few iterations. The readers should keep in mind that these iteration are very inexpensive.

3. (a) Given the displacement of the rigid object, use it to set the boundary conditions for the fluid mesh motion problem as:

$$\hat{\mathbf{d}}_{n+1,(l)} = (\mathbf{Q}_{n+1,(l)} - \mathbf{I})(\mathbf{X} - \mathbf{X}_0) + (\mathbf{d}_0)_{n+1,(l)} \quad (64)$$

(b) Evaluate the intermediate time level mesh displacement as:

$$\hat{\mathbf{d}}_{n+\alpha_f,(l)} = \hat{\mathbf{d}}_n + \alpha_f (\hat{\mathbf{d}}_{n+1,(l-1)} - \hat{\mathbf{d}}_n) \quad (65)$$

(c) Use the intermediate mesh displacement solution to assemble  $\mathbf{R}^{mesh}$ , the discrete residual of the mesh motion problem, and the corresponding left-hand side matrix of the linear equation system:

$$\frac{\partial \mathbf{R}^{mesh}}{\partial \hat{\mathbf{u}}_{n+1}} \Delta \hat{\mathbf{u}} = -\mathbf{R}_{(l)}^{mesh} \quad (66)$$

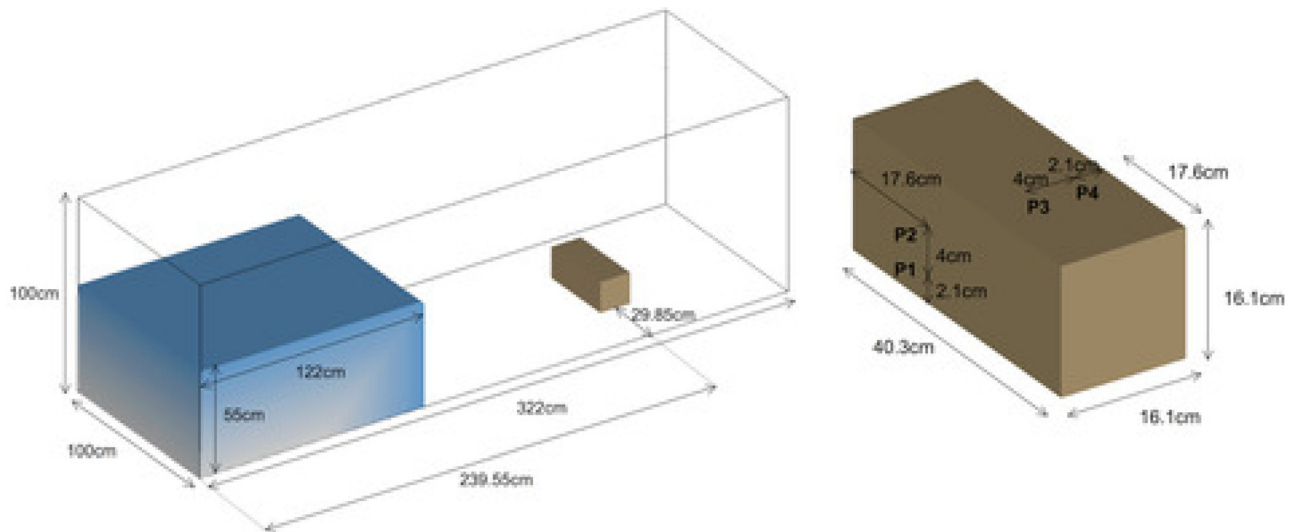
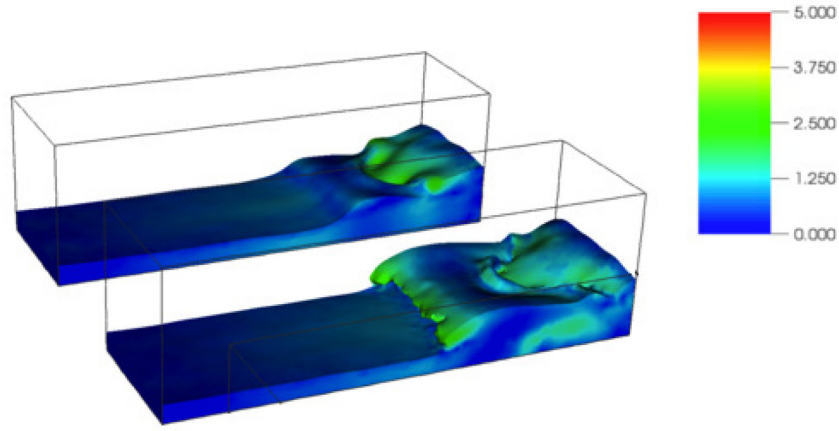


Fig. 2 Dam break with obstacle. Problem setup.



**Fig. 3 Dam break with obstacle. Snapshots of the water subdomain colored by the fluid speed at  $t = 2.0$  s. Top: solution without penalty. Bottom: solution with  $\lambda_{pen} = 1$ .**

Solve this linear system using a preconditioned Conjugate Gradient algorithm to a specified tolerance.

(d) Update the mesh motion solution as:

$$\begin{aligned}\hat{\mathbf{u}}_{n+1,(l)} &= \hat{\mathbf{u}}_{n+1,(l)} + \Delta \hat{\mathbf{u}} \\ \hat{\mathbf{u}}_{n+1,(l)} &= \hat{\mathbf{u}}_{n+1,(l)} + \gamma \Delta t \Delta \hat{\mathbf{u}} \\ \hat{\mathbf{d}}_{n+1,(l)} &= \hat{\mathbf{d}}_{n+1,(l)} + \beta \Delta t^2 \Delta \hat{\mathbf{u}}\end{aligned}\quad (67)$$

**Level Set Correction Stage.** Re-distance the level set field according to Eq. (22) and correct for mass deficit according to Eq. (27).

This completes the time step, at which point the time step counter is incremented and we go back to the predictor stage.

Remark. Our rigid body time integration algorithm amounts to applying the midpoint rule to Eqs. (48) and (49) as well as Eq. (41). That is, the rotation matrix  $\mathbf{Q}$  is not explicitly computed from the rotation angles, but is carried as a separate problem unknown. The choice of the midpoint time integration for Eq. (41) results in the following remarkable property: if  $\mathbf{Q}_n^T \mathbf{Q}_n = \mathbf{Q}_n \mathbf{Q}_n^T = \mathbf{I}$  then  $\mathbf{Q}_{n+1}^T \mathbf{Q}_{n+1} = \mathbf{Q}_{n+1} \mathbf{Q}_{n+1}^T = \mathbf{I}$ . That is, once ini-

tialized as a proper rotation matrix,  $\mathbf{Q}$  remains a proper rotation matrix during the entire simulation. This result is due to Ref. [44].

## 5 Numerical Results

In this section, we present two numerical examples. The first one is the well-known MARIN dam break problem [14–17], which is a free-surface flow without fluid-object interaction. The problem is solved on a fixed mesh and is used to illustrate the effect of the penalty term in the re-distancing step given by Eq. (25). This problem is also used to compare a fully-coupled versus staggered approach to level set convection. The second example makes use of a DTMB 5415 Navy combatant at lab scale in head waves of large amplitude.

**5.1 Dam Break With Obstacle.** The problem consists of a  $1.22\text{ m} \times 1\text{ m} \times 0.55\text{ m}$  column of water, initially at rest, that collapses under the action of gravity and impacts a stationary object. The computational domain is a rectangular box with dimensions  $3.22\text{ m} \times 1\text{ m} \times 1\text{ m}$ . The object has dimensions

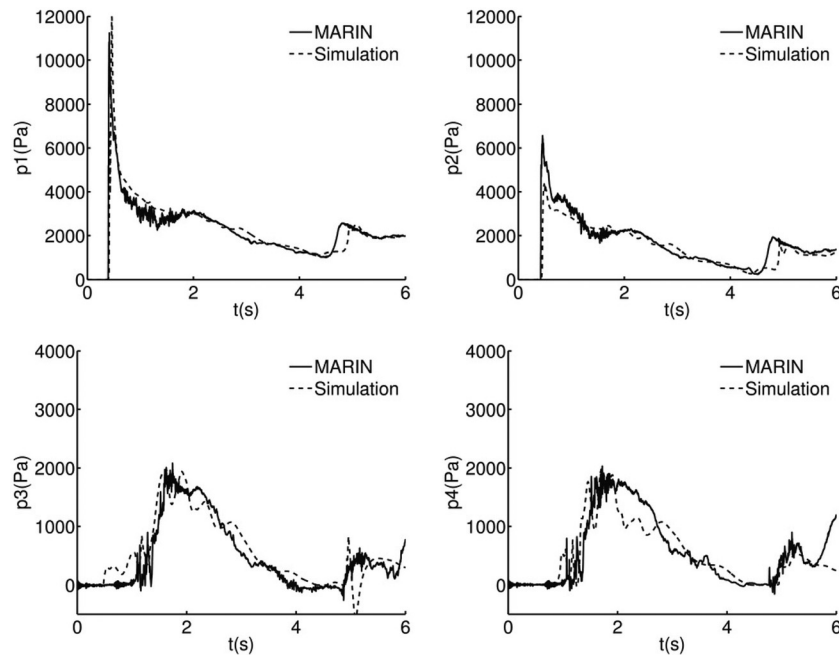


**Fig. 4 Dam break with obstacle. Time series of the pressure at four locations on the obstacle (see Fig. 2). Very close correlation with experimental data is obtained.**

$0.161\text{ m} \times 0.161\text{ m} \times 0.403\text{ m}$  and is placed at the back end of the tank. The problem setup is shown in Fig. 2. Experiments for this test case were performed at the Maritime Research Institute Netherlands (MARIN), and the data is often used to validate free-surface software for marine engineering applications.

In Refs. [14,15] we computed this test case with linear hexahedral and quadratic NURBS and reported very good correlation between experimental and computational results. In this paper, we employ linear tetrahedral elements and use the MARIN example to assess the influence of the penalty parameter in the re-distancing equations, and illustrate the increased robustness of the direct coupling between the fluid flow and level set equations.

**5.1.1 Influence of Penalty in the Re-Distancing.** Simulations with two different penalty parameters,  $\lambda_{pen}=0$ ,  $\lambda_{pen}=1$ , are performed on a mesh consisting of 344,401 tetrahedral elements and 60,797 nodes. The simulation was run until  $T=6.0\text{ s}$  with a time step of  $\Delta t=0.01$ . Snapshots of the solution for both simulations are shown in Fig. 3. At  $t=2.0\text{ s}$ , the water has already hit the obstacle and rebounded off the back wall of the tank to form a breaking wave. The case with penalty shows a crisp resolution of the air-water interface and is correctly predicting the formation of a breaking wave. The no-penalty case, however, produced an over-diffuse interface and; as a result, it is unable to predict wave breaking. This example clearly illustrates the fact that the regularized sign function given by Eq. (24) is not a sufficient mechanism by itself to keep the interface intact during re-distancing.

Figure 4 shows the pressure history on four different locations on the obstacle. The simulated results correlate quite well with the experiments for such a coarse discretization.

**5.1.2 Fully-Coupled Versus Staggered Fluid-Level Set Simulations.** Here we solve a MARIN dam break problem using the solution strategy presented in Sec. 4 and compare it with the solution strategy we presented in Refs. [14,15]. The latter decouples the Navier-Stokes and level set convection equations and performs one convection step, which includes re-distancing and mass correction, at the end of the time step. This methodology is commonly used in free surface computations reported in the literature. For this test, we reduce the mesh size to 103 251 tetrahedral elements and 19 071 nodes. We increase the time step size to  $\Delta t=0.025$  and compute the problem until  $T=12.5\text{ s}$ . By this time, the fluid solution should be well on its way to a steady result. Figure 5 shows the fluid solution at  $t=12.5\text{ s}$ , the final time. The fully coupled strategy gives a physical, near steady-state result, while the staggered case predicts large-magnitude sloshing, which is unphysical. This is due to the large time step size that triggers an instability in the simulations. This example illustrates the danger of using staggered methods with time step sizes that exceed

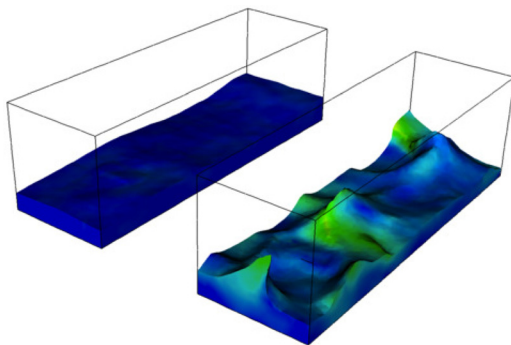


**Fig. 5** Dam break with obstacle. Snapshots of the water subdomain colored by the fluid speed at  $t=12.5\text{ s}$ . Top: fully coupled simulation. Bottom: staggered simulation. For the chosen time step size, the coupled simulation produces a physical, near steady-state result, while the staggered approach gives unphysical, large-magnitude sloshing.

the stability limits of the formulation and lead to seemingly convergent, yet completely unphysical results.

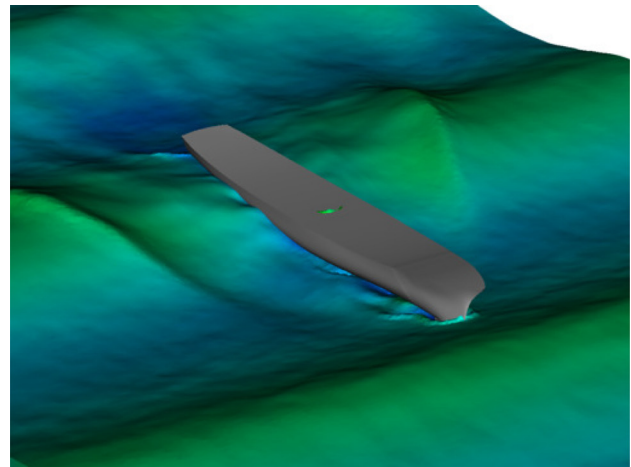
**5.2 Ship in Head Sea.** Here we simulate the DTMB 5415 Navy combatant at lab scale. This ship has been investigated by other researchers, both experimentally and computationally (see Refs. [45–47]). The length of the ship hull is  $5.72\text{ m}$ . The ship mass, center of gravity and inertia tensor are computed by meshing the ship interior and performing a direct computation. The total ship volume is  $1.366\text{ m}^3$ . The ship mass is equal to  $532.3\text{ kg}$ . It is obtained by multiplying the volume of the ship below the water line by the constant water density. The center of gravity and the inertia tensor are computed assuming the ship's effective density (i.e., the ship mass divided by its total volume), which results in

$$\mathbf{X}_0 = \begin{bmatrix} 2.761\text{ m} \\ 0 \\ 0.280\text{ m} \end{bmatrix} \quad (68)$$

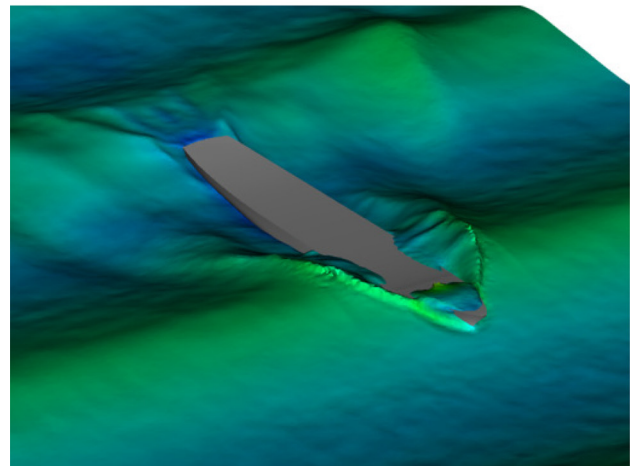
and

$$\mathbf{I} = \begin{bmatrix} 7.256\text{E}-2 & 2.69\text{E}-7 & 5.35\text{E}-2 \\ 2.69\text{E}-7 & 2.89 & -2.44\text{E}-8 \\ 5.35\text{E}-2 & -2.44\text{E}-8 & 2.91 \end{bmatrix} \text{ kg m}^2 \quad (69)$$

respectively.



(a)  $t=9.00\text{ s}$



(b)  $t=9.50\text{ s}$

**Fig. 6** DTMB 5415 in head sea. Snapshots of the ship negotiating high-amplitude waves. The water surface is colored by the fluid speed.

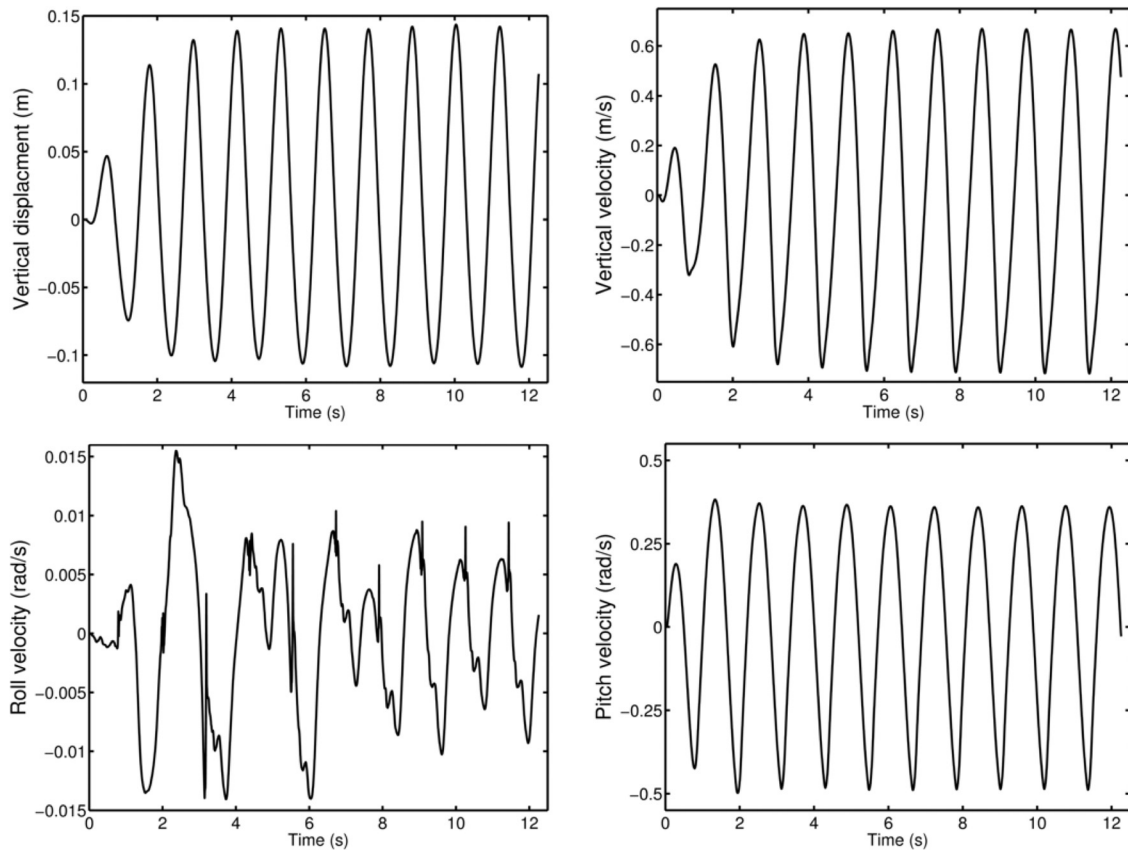


Fig. 7 DTMB 5415 in head sea. Time history of ship motion.

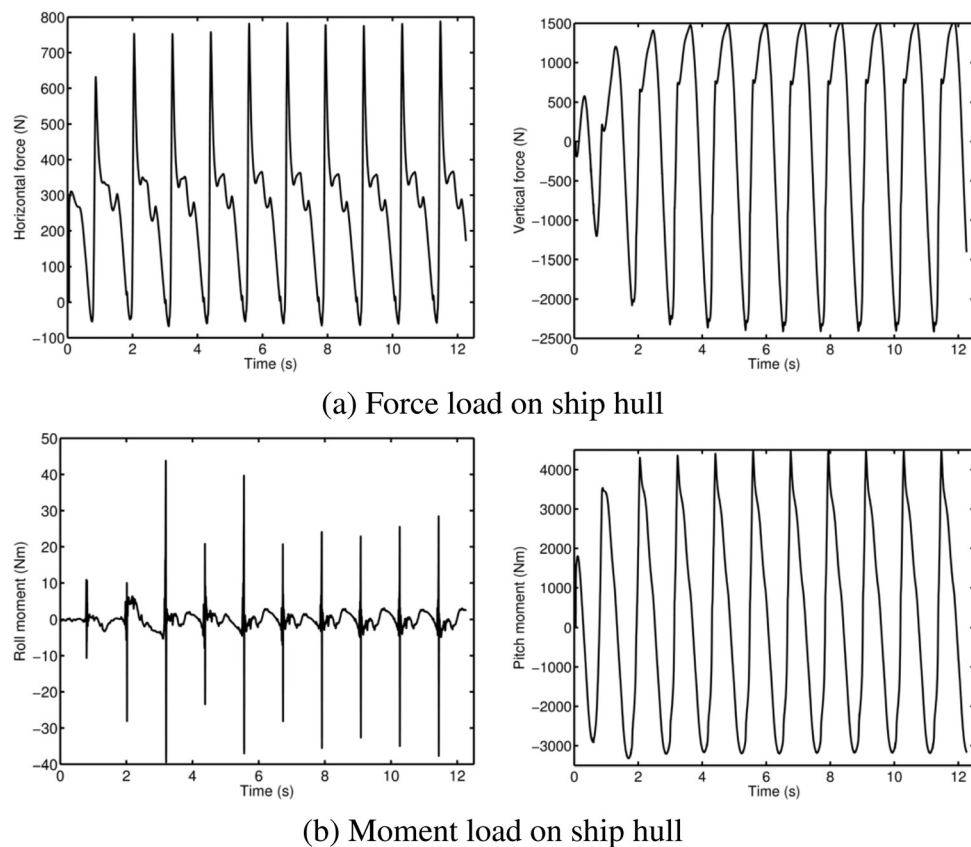


Fig. 8 DTMB 5415 in head sea. Time history of forces and moments acting on the ship.

We compute the ship in head waves, meaning the waves that travel in the direction opposite to that of the ship. We assume that the ship speed is  $U_{in} = 1.873 \text{ m/s}$ , which gives the Froude number of 0.25 based on the ship length.

We make use of the linear Airy waves [48] to prescribe inlet boundary conditions. The Airy waves may be derived using potential theory, and are specified as follows: Given, the wave amplitude, wave length and water depth,  $A_w = 0.2 \text{ m}$ ,  $L_w = 5.72 \text{ m}$  and  $h = 3.49 \text{ m}$ , respectively, we compute  $k = 2\pi/L_w$ , the angular wavenumber,  $\omega = \sqrt{gk \tanh(kh)}$ , the wave phase speed, and  $A_v = \frac{\omega A_w}{\sinh(kh)}$ , the velocity amplitude. With these definitions, the Airy waves are given by:

$$u = A_v \cosh(kz) \cos(kx - \omega t) + U_{in} \quad (70)$$

$$v = 0 \quad (71)$$

$$w = A_v \sinh(kz) \sin(kx - \omega t) \quad (72)$$

$$\phi = A_w \cos(kx - \omega t) + h - z \quad (73)$$

where  $\mathbf{u} = (u, v, w)$  is the fluid velocity vector and the air-water interface in the hydrostatic configuration is assumed to be located at  $z = 0$ .

In the continuum setting, the fluid traction vector  $\mathbf{h}$  is defined as:

$$\mathbf{h} = p\mathbf{n} - 2\mu\nabla^s \mathbf{u} \cdot \mathbf{n} \quad (74)$$

In the discrete setting, in the presence of weakly-enforced boundary conditions, basic conservation arguments (see Ref.[49]) lead to the following definition of the traction vector

$$\mathbf{h} = p^h \mathbf{n} - 2\mu\nabla^s \mathbf{u}^h \cdot \mathbf{n} + \tau_B(\mathbf{u}^h - \mathbf{d}) \quad (75)$$

We use this definition of  $\mathbf{h}$  for the computation of global force and moment vectors (see Eqs. (46) and (47)) acting on the ship hull.

The simulation was performed on a mesh consisting of 6 285 445 linear tetrahedral elements and 1 059 174 nodes. The simulation took 5000 time steps at a fixed time step size of  $\Delta t = 0.0025 \text{ s}$ . The ship was allowed to move vertically, to pitch and to roll, while the rest of the rigid body DOFs were constrained.

Figure 6 shows the snapshots of the ship negotiating high-amplitude waves. The bottom part of Fig. 6 shows the ship partially submerged in water, which is a result of the oncoming wave hitting the bow of the ship. In this case, near the bow, the free surface experiences topological changes, which necessitates the use of an interface-capturing method for this class of problems.

The time history of the ship motion is given in Fig. 7. Although the prescribed Airy waves only have a single frequency, multiple frequencies are present in the ship's response. Note that the ship develops a low-amplitude, chaotic rolling motion.

Figure 8(a) shows the time history of the thrust force necessary to maintain the ship moving forward at constant speed. The time history of the forces and moments in the unconstrained directions are shown in Figs. 8(b)–(d).

## 6 Conclusions

A free surface-rigid-body interaction modeling approach is presented using the MITICT approach, in which the air-water interface is handled by means of an interface-capturing level set method, and the fluid-rigid body interface is handled with an interface-tracking ALE method. The RBVMS formulation is used for the fluid mechanics and level set equations. Weak enforcement of essential boundary conditions is employed on all no-slip surfaces for better approximation of thin fluid boundary layers. The rigid-body time integration algorithm is proposed where a separate time evolution equation is solved for the rotation matrix, which becomes an additional problem unknown. The use of the

midpoint time integration algorithm for the rotation matrix results in the exact discrete preservation of its orthonormal property, a result that is due to Ref. [44]. In the proposed methodology, the strong coupling between the fluid and level set equations at the Newton iteration level allows us to robustly march in time by using larger time-steps than in the more usual staggered (or split operator) methods. We also illustrate the importance of the penalty parameter in the level set re-distancing equations for the preservation of the sharpness of the air-water interface.

In future work, we plan to enhance the structural modeling in our framework by also considering elastic bodies. We likewise plan to simulate ships at larger spatial scales, and look at other applications, such as modeling of offshore wind turbines.

## Acknowledgment

This research was supported in part by an appointment to the Postgraduate Research Participation Program at the U.S. Army Engineering Research and Development Center, Coastal and Hydraulics Laboratory (ERDC-CHL) administered by the Oak Ridge Institute for Science and Education through an interagency agreement between the U.S. Department of Energy and ERDC. The corresponding author was supported through ARO Award W911NF-11-1-0083. Permission was granted by the Chief of Engineers to publish this information.

## References

- [1] Takizawa, K., Tanizawa, K., Yabe, T., and Tezduyar, T., 2007, "Ship Hydrodynamics Computations With the CIP Method Based on Adaptive Soroban Grids," *Int. J. Numer. Methods Fluids*, **54**, pp. 1011–1019.
- [2] Tezduyar, T., Aliabadi, S., and Behr, M., 1998, "Enhanced-Discretization Interface-Capturing Technique (EDICT) for Computation of Unsteady Flows With Interfaces," *Comput. Methods Appl. Mech. Eng.*, **155**, pp. 235–248.
- [3] Sethian, J., 1999, *Level Set Methods and Fast Marching Methods*, Cambridge University Press, London.
- [4] Sussman, M., Smereka, P., and Osher, S., 1994, "A Level Set Approach for Computing Solutions to Incompressible Two-Phase Flows," *J. Comput. Phys.*, **114**, pp. 146–159.
- [5] Nagrath, S., Jansen, K., and Lahey, R., 2005, "Computation of Incompressible Bubble Dynamics With a Stabilized Finite Element Level Set Method," *Comput. Methods Appl. Mech. Eng.*, **194**, pp. 4565–4587.
- [6] Olsson, E., and Kreiss, G., 2005, "A Conservative Level Set Method for Two Phase Flow," *J. Comput. Phys.*, **210**, pp. 225–246.
- [7] Tezduyar, T., 2001, "Finite Element Methods for Flow Problems With Moving Boundaries and Interfaces," *Arch. Comput. Methods Eng.*, **8**, pp. 83–130.
- [8] Akin, J., Tezduyar, T., and Ungor, M., 2007, "Computation of Flow Problems With the Mixed Interface-Tracking/Interface-Capturing Technique (MITICT)," *Comput. Fluids*, **36**, pp. 2–11.
- [9] Tezduyar, T., Behr, M., and Liou, J., 1992, "A New Strategy for Finite Element Computations Involving Moving Boundaries and Interfaces—The Deforming-Spatial-Domain/Space-Time Procedure: I. The Concept and the Preliminary Numerical Tests," *Comput. Methods Appl. Mech. Eng.*, **94**(3), pp. 339–351.
- [10] Tezduyar, T., Behr, M., Mittal, S., and Liou, J., 1992, "A New Strategy for Finite Element Computations Involving Moving Boundaries and Interfaces—The Deforming-Spatial-Domain/Space-Time Procedure: II. Computation of Free-Surface Flows, Two-Liquid Flows, and Flows With Drifting Cylinders," *Comput. Methods Appl. Mech. Eng.*, **94**(3), pp. 353–371.
- [11] Cruchaga, M., Celentano, D., and Tezduyar, T., 2007, "A Numerical Model Based on the Mixed Interface-Tracking/Interface-Capturing Technique (MITICT) for Flows With Fluid-Solid and Fluid-Fluid Interfaces," *Int. J. Numer. Methods Fluids*, **54**, pp. 1021–1031.
- [12] Cruchaga, M., Celentano, D., and Tezduyar, T., 2001, "A Moving Lagrangian Interface Technique for Flow Computations Over Fixed Meshes," *Comput. Methods Appl. Mech. Eng.*, **191**, pp. 525–543.
- [13] Hughes, T. J. R., Liu, W. K., and Zimmermann, T. K., 1981, "Lagrangian-Eulerian Finite Element Formulation for Incompressible Viscous Flows," *Comput. Methods Appl. Mech. Eng.*, **29**, pp. 329–349.
- [14] Kees, C., Akkerman, I., Farthing, M., and Bazilevs, Y., 2011, "A Conservative Level Set Method Suitable for Variable-Order Approximations and Unstructured Meshes," *J. Comput. Phys.*, **230**, pp. 4536–4558.
- [15] Akkerman, I., Bazilevs, Y., Kees, C., and Farthing, M., 2011, "Isogeometric Analysis of Free-Surface Flow," *J. Comput. Phys.*, **230**, pp. 4137–4152.
- [16] Kleefsman, K., Fekken, G., Veldman, A., Iwanowski, B., and Buchner, B., 2005, "A Volume-of-Fluid Based Simulation Method for Wave Impact Problems," *J. Comput. Phys.*, **206**, pp. 363–393.
- [17] Elias, R., and Coutinho, A., 2007, "Stabilized Edge-Based Finite Element Simulation of Free-Surface Flows," *Int. J. Numer. Methods Fluids*, **54**, pp. 965–993.

- [18] Lins, E. F., Elias, R. N., Rochinha, F. A., and Coutinho, A. L. G. A., 2010, "Residual-Based Variational Multiscale Simulation of Free Surface Flows," *Comput. Mech.*, **46**, pp. 545–557.
- [19] Bazilevs, Y., Calo, V., Cottrell, J., Hughes, T. J. R., Reali, A., and Scovazzi, G., 2007, "Variational Multiscale Residual-Based Turbulence Modeling for Large Eddy Simulation of Incompressible Flows," *Comput. Methods Appl. Mech. Eng.*, **197**, pp. 173–201.
- [20] Bazilevs, Y., Calo, V., Zhang, Y., and Hughes, T. J. R., 2006, "Isogeometric Fluid-Structure Interaction Analysis With Applications to Arterial Blood Flow," *Comput. Mech.*, **38**, pp. 310–322.
- [21] Akkerman, I., Bazilevs, Y., Calo, V., Hughes, T. J. R., and Hulshoff, S., 2008, "The Role of Continuity in Residual-Based Variational Multiscale Modeling of Turbulence," *Comput. Mech.*, **41**, pp. 371–378.
- [22] Bazilevs, Y., Michler, C., Calo, V., and Hughes, T. J. R., 2007, "Weak Dirichlet Boundary Conditions for Wall-Bounded Turbulent Flows," *Comput. Methods Appl. Mech. Eng.*, **196**, pp. 4853–4862.
- [23] Bazilevs, Y., Michler, C., Calo, V., and Hughes, T. J. R., 2010, "Isogeometric Variational Multiscale Modeling of Wall-Bounded Turbulent Flows With Weakly-Enforced Boundary Conditions on Unstretched Meshes," *Comput. Methods Appl. Mech. Eng.*, **199**(13–16), pp. 780–790.
- [24] Bazilevs, Y., Gohean, J., Hughes, T. J. R., Moser, R., and Zhang, Y., 2009, "Patient-Specific Isogeometric Fluid-Structure Interaction Analysis of Thoracic Aortic Blood Flow Due to Implantation of the Jarvik 2000 Left Ventricular Assist Device," *Comput. Methods Appl. Mech. Eng.*, **198**, pp. 3534–3550.
- [25] Bazilevs, Y., Calo, V., Hughes, T. J. R., and Zhang, Y., 2008, "Isogeometric Fluid-Structure Interaction: Theory, Algorithms, and Computations," *Comput. Mech.*, **43**, pp. 3–37.
- [26] Hsu, M., Bazilevs, Y., Calo, V., Tezduyar, T., and Hughes, T. J. R., 2010, "Improving Stability of Multiscale Formulations of Fluid Flow at Small Time Steps," *Comput. Methods Appl. Mech. Eng.*, **199**, pp. 828–840.
- [27] Bazilevs, Y., Hsu, M.-C., Akkerman, I., Wright, S., Takizawa, K., Henicke, B., Spielman, T., and Tezduyar, T., 2011, "3D Simulation of Wind Turbine Rotors at Full Scale. Part I: Geometry Modeling and Aerodynamics," *Int. J. Numer. Methods Fluids*, **65**, pp. 207–235.
- [28] Bazilevs, Y., Hsu, M.-C., Kiendl, J., Wuechner, R., and Bletzinger, K.-U., 2011, "3D Simulation of Wind Turbine Rotors at Full Scale. Part II: Fluid-Structure Interaction," *Int. J. Numer. Methods Fluids*, **65**, pp. 236–253.
- [29] Bazilevs, Y., and Hughes, T. J. R., 2007, "Weak Imposition of Dirichlet Boundary Conditions in Fluid Mechanics," *Comput. Fluids*, **36**, pp. 12–26.
- [30] Brooks, A., and Hughes, T. J. R., 1982, "Streamline Upwind/Petrov-Galerkin Formulations for Convection Dominated Flows With Particular Emphasis on the Incompressible Navier–Stokes Equations," *Comput. Methods Appl. Mech. Eng.*, **32**, pp. 199–259.
- [31] Harari, I., and Hughes, T. J. R., 1992, "What are C and h?: Inequalities for the Analysis and Design of Finite Element Methods," *Comput. Methods Appl. Mech. Eng.*, **97**, pp. 157–192.
- [32] Tezduyar, T., 2004, "Finite Element Methods for Fluid Dynamics With Moving Boundaries and Interfaces," *Encyclopedia of Computational Mechanics*, E. Stein, R. D. Borst, and T. J. R. Hughes, eds., Vol. 3: Fluids, John Wiley & Sons, New York.
- [33] Tezduyar, T., and Senga, M., 2006, "Stabilization and Shock-Capturing Parameters in SUPG Formulation of Compressible Flows," *Comput. Methods Appl. Mech. Eng.*, **195**, pp. 1621–1632.
- [34] Galeao, A., and do Carmo, E. D., 1988, "A Consistent Approximate Upwind Petrov–Galerkin Method for Convection-Dominated Problems," *Comput. Methods Appl. Mech. Eng.*, **68**(1), pp. 83–95.
- [35] Rispoli, F., Corsini, A., and Tezduyar, T., 2007, "Finite Element Computation of Turbulent Flows With the Discontinuity-Capturing Directional Dissipation (DCDD)," *Comput. Fluids*, **36**, pp. 121–126.
- [36] Tezduyar, T., Ramakrishnan, S., and Sathe, S., 2008, "Stabilized Formulations for Incompressible Flows With Thermal Coupling," *Int. J. Numer. Methods Fluids*, **57**, pp. 1189–1209.
- [37] Tezduyar, T., and Osawa, Y., 2000, "Finite Element Stabilization Parameters Computed From Element Matrices and Vectors," *Comput. Methods Appl. Mech. Eng.*, **190**, pp. 411–430.
- [38] Tezduyar, T., 2003, "Computation of Moving Boundaries and Interfaces and Stabilization Parameters," *Int. J. Numer. Methods Fluids*, **43**, pp. 555–575.
- [39] John, V., and Knobloch, P., 2007, "On Spurious Oscillations at Layers Diminishing (Sold) Methods for Convection-Diffusion Equations: Part I—A review," *Comput. Methods Appl. Mech. Eng.*, **196**(17–20), pp. 2197–2215.
- [40] Stein, K., Tezduyar, T., and Benney, R., 2003, "Mesh Moving Techniques for Fluid-Structure Interactions With Large Displacements," *J. App. Mech.*, **70**, pp. 58–63.
- [41] Chung, J., and Hulbert, G. M., 1993, "A Time Integration Algorithm for Structural Dynamics With Improved Numerical Dissipation: The Generalized- $\alpha$  Method," *J. App. Mech.*, **60**, pp. 371–375.
- [42] Jansen, K. E., Whiting, C. H., and Hulbert, G. M., 1999, "A Generalized- $\alpha$  Method for Integrating the Filtered Navier–Stokes Equations With a Stabilized Finite Element Method," *Comput. Methods Appl. Mech. Eng.*, **190**, pp. 305–319.
- [43] Saad, Y., and Schultz, M., 1986, "GMRES: A Generalized Minimal Residual Algorithm for Solving Non-Symmetric Linear Systems," *SIAM J. Sci. Comput.*, **7**, pp. 856–869.
- [44] Hughes, T. J. R., and Winget, J., 1980, "Finite Rotation Effects in Numerical Integration of Rate Constitutive Equations Arising in Large-Deformation Analysis," *Int. J. Numer. Methods Eng.*, **15**, pp. 1862–1867.
- [45] Longo, J., and Stern, F., 2005, "Uncertainty Assessment for Towing Tank Tests With Example for Surface Combatant DTMB Model 5415," *J. Ship Res.*, **49**, pp. 55–68.
- [46] Garcia, J., and Oñate, E., 2003, "An Unstructured Finite Element Solver for Ship Hydrodynamics Problems," *J. App. Mech.*, **70**, pp. 18–26.
- [47] Longo, J., Shao, J., Irvine, M., and Stern, F., 2007, "Phase-Averaged PIV for the Nominal Wake of a Surface Ship in Regular Head Waves," *J. Fluids Eng.*, **129**, pp. 524–541.
- [48] McCormick, M., 2010, *Ocean Engineering Mechanics. With Applications*, Cambridge University Press, London.
- [49] Bazilevs, Y., and Akkerman, I., 2010, "Large Eddy Simulation of Turbulent Taylor–Couette Flow Using Isogeometric Analysis and the Residual-Based Variational Multiscale Method," *J. Comput. Phys.*, **229**(9), pp. 3402–3414.